Available online at www.sciencedirect.com
SCIENCE DIRECT®
International Journal of Solids and Structures 42 (2005) 2711–2739
INTERNATIONAL JOURNAL OF SOLIDS and STRUCTURES
www.elsevier.com/locate/ijsolstr

A solution including skin effect for stiffness and stress field of sandwich honeycomb core

An Chen, Julio F. Davalos *

Department of Civil and Environmental Engineering, West Virginia University, 611C Engineering Science Building, Morgantown, WV 26506-6103, USA

Received 7 May 2004; received in revised form 27 September 2004
Available online 6 November 2004

Abstract

Honeycomb sandwich panels have been increasingly used in every possible field, and their efficient load carrying capacity attributes have attracted considerable attention. All previous studies have been focused mainly on stiffness, neglecting for the most part skin effects. This paper represents an important further contribution by developing an analytical model that permits the computation of stiffnesses as well as interfacial stresses considering the skin-effect for hexagonal honeycomb sandwich, subjected to in-plane and out-of-plane forces. An explicit analytical model is derived based on equilibrium equations, where boundary conditions imposed by the skin effect are appropriately considered. The accuracy of the solution is verified through close correlations with existing stiffness formulations and finite element results. The skin effect on both stiffness and interfacial stress distribution is analytically defined. The present model is then used to carry out a parametric study on interfacial stresses, and to detect the critical sections in the structure where further consideration should be given for design purposes. The method provided in this study can be used for accurate analysis and design of sandwich structures.

Keywords: Sandwich honeycomb panel; Skin effect; Stress distribution; Explicit solution; Finite element analysis; Parametric study

1. Introduction

A typical sandwich panel is made of two stiff skins, separated by a lightweight honeycomb core. It may be designed so that each component is utilized to its ultimate limit. This feature makes sandwich structures

* Corresponding author. Address: Department of Civil and Environmental Engineering, West Virginia University, 611C Engineering Science Building, Morgantown, WV 26506-6103, USA. Tel.: +1 304 293 3031x2632; fax: +1 304 293 7109.
E-mail address: jfdavalos@mail.wvu.edu (J.F. Davalos).

0020-7683/$ - see front matter © 2004 Elsevier Ltd. All rights reserved.
doi:10.1016/j.ijsolstr.2004.09.042

attractive in various engineering fields where stiffness and strength must be met with minimum weight (Vinson, 1999). The concept of sandwich construction has been traced back to the mid 19th century (Fairbairn, 1849), while the broad introduction of the sandwich concept in aircraft structures started at the beginning of World War II. Nowadays sandwich panels and shells have been widely used in aerospace, shipbuilding, civil infrastructure and other industries (Davalos et al., 2001).

Conventionally hexagonal honeycomb sandwiches (see Fig. 1) have been applied in the aerospace industry since the 1940's, and have been increasingly used in every possible field. The commonly used core materials include aluminum, alloys, titanium, stainless steel, and polymer composites. Apparently, the computational models on honeycomb sandwiches are generally based on the equivalent replacement of each component with homogeneous continuum, due to expensive computation of 3-D detailed properties. Therefore, to accurately represent the equivalent properties has been a perennial challenging topic that attracted a lot of investigations. From Fig. 1, one can intuitively conclude that honeycomb sandwich structures behave like I-beams: the outer facesheets correspond to the flanges, and carry most of the direct compression/tension bending load, and the lightweight core corresponds to the I-beam web. The core supports the skins, increases bending and torsional stiffness, and carries most of the shear load (Noor et al., 1996). This characteristic of a three-layer arrangement leads to classical sandwich theory (Allen, 1969; Zenkert, 1995). Unlike the facesheet, which can even be a laminated plate, the equivalent properties of honeycomb cores are more complicated. A lot of research has been devoted to this area. These include Warren and Kraynik (1987), Gibson and Ashby (1988), Fortes and Ashby (1999), and included in the book of Gibson and Ashby (1988) is the first systematic literature review in the field. All these mathematical models are based on pure cellular structures and the presence of the facesheet is not considered. As a result, the existing analytical solutions do not agree well with experimental results (Shi and Tong, 1995).

In order to more accurately describe the elastic moduli of the core, Penzien and Didriksson (1964) introduced the concept of warping effect, or skin effect, into the model. Later Grediac (1993), Shi and Tong (1995), Becker (1998), and Xu and Qiao (2002) further considered this effect in their studies. It is interesting to point out that different researchers defined this effect in different ways, such as warping constraint by Penzien and Didriksson (1964), thickness effect by Becker (1998), bending effect by Grediac (1993), and skin effect by Xu and Qiao (2002). Recently Chen and Davalos (2004) decomposed this effect into shear and bending warping effects. However, all of these studies, either using 2-D model or finite element (FE) method, were focused on the stiffness study only, and no work is available on the stress distribution at the interface, partly due to the following reasons: (1) the skin effect introduces a complicated stress field

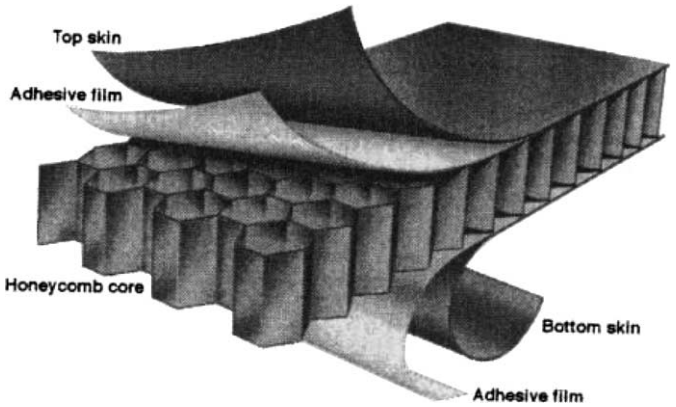

Fig. 1. Sandwich panel with hexagonal honeycomb core (from Noor et al., 1996).

at the interface, which is difficult to model; and (2) unlike the modelling of stress distribution, acceptable results can be obtained for stiffness, which is a global property, even if an approximate displacement function is assumed.

Several studies (e.g., Chen and Davalos, 2003) have shown that delamination of the core from facesheet is a typical failure mode for sandwich panels. Since stress concentration can act as a criterion to predict the onset of the delamination, there is a need to further investigate stress field at the interface. Therefore, the aim of this study is to present an analytical model allowing the calculation of the stiffness of honeycomb cores as well as the interfacial stress distribution considering skin effect, both under in-plane and out-of-plane forces. The present results obtained constitute upper limits of actual values, since the commonly used rigid facesheet assumption is also adopted in this study, which neglects the bending stiffness contributions of actual facesheets.

2. Literature review

A comprehensive review of the computational models on honeycomb sandwiches was given by Noor et al. (1996), where numerous references were cited. Xu and Qiao (2002) provided a review specifically on stiffness studies of hexagonal honeycomb core. Basically, all existing studies can be organized into two groups.

2.1. Neglecting skin effect

The practice of neglecting skin effect is prevalent in today's sandwich research and design, wherein a uniform stress distribution in the walls of the structure is assumed. The in-plane elastic properties were first obtained by Gibson and Ashby (1988), where conditions of uni-axial loading and bi-axial loading were considered. Masters and Evans (1996) further refined the analysis attempting to consider stretching and hinging effects. Kelsey et al. (1958) firstly applied energy method to calculate the transverse shear stiffness, and showed that the theory of minimum potential energy, a kinematically compatible uniform strain field, gives an upper bound; and the theory of complementary energy, a statically compatible uniform stress field, gives a lower bound, corresponding to zero and infinitely large skin effect, respectively. The expressions for these two bounds were provided in terms of unit load and unit displacement method. Gibson and Ashby (1988) presented the predictions for transverse shear stiffness using mechanics of materials and energy method. In parallel to energy method, a good attempt was made by Shi and Tong (1995) in presenting an analytical solution for hexagonal honeycomb core using a 2-D homogenization method and obtaining the lower bound value. Xu et al. (2001) further extended it to general honeycomb configurations, where they developed an analytical approach with a two-scale asymptotic homogenization method.

2.2. Considering skin effect

As observed in experiments (Adams and Maheri, 1993; Daniel and Abot, 2000), skin constrain was demonstrated by the phenomenon of skin lateral contraction and expansion. Rather than assuming a uniform stress field, Penzien and Didriksson (1964) formulated a displacement field for transverse shear problem to simulate the warping effect induced by the facesheet. For the first time they showed the trend that as core height increases, the transverse shear stiffness decreases. Recently Xu and Qiao (2002) applied a multi-pass homogenization method to study the stiffness for transverse shear, in-plane stretch and out-of-plane

bending. In both of these studies, the inclined panel was unfolded into the plane of flat panel, and therefore, the solution corresponds to a 2-D model. Grediac (1993) applied FE method to study core cells with different core configurations, and he studied the stress distribution in core walls. He concluded that the skin effect is a localized phenomenon limited only to the region adjacent to the interface. However, due to the cumbersome modelling work required by FE analysis, his study was only case-specific and not applicable to carry out general parametric studies.

Unlike the equivalent shear stiffness of honeycomb core, the skin effect on other stiffness components received less attention. The only literature that could be found on equivalent in-plane moduli considering skin effect was the work by Becker (1998). He derived a closed-form solution to predict the in-plane moduli and compared them with FE results. However, his solution is implicit, making it difficult for practical use. A further expansion was attempted recently by Hohe and Becker (2001a) to include all stiffness components for general honeycomb cores, but still using implicit calculations.

Burton and Noor (1997) used detailed FE models to examine the effect of the adhesive joint on the load transfer and static responses of sandwich panels. However, they used strain energy for discrete components to discuss the effect of various parameters, a method which does not consider delamination. Through a rigorous asymptotic analysis, Hohe et al. (2001b) provided a solution to the stress fields in the cell walls of hexagonal honeycomb cores in the form of a power-law function. They pointed out that the stress singularity occurs at the intersection of the cell walls at the core facesheet interface. Considering the stress concentration and singularity due to deformation incompatibility associated with the facesheets and cellular core, they used a continuum mechanics method to assess the delamination hazard by the skin effect (Hohe and Becker, 2001c). They concluded that the additional strain energy release, which is caused by skin effect, controls the nucleation and growth of microcracks which lead to large scale delamination at a later stage. However, in both of the above analytical studies, the displacement function was pre-defined, either using a power-law function (Hohe et al., 2001b) or hyperbolic cosine function (Hohe and Becker, 2001c), without direct physical meanings. Therefore, it is advantageous to develop a method based on basic equilibrium equations to calculate the stiffness as well as the interfacial stresses, which is the motivation of this study.

3. Objectives and scope

Due to their extensive industrial application, the immediate focus of this study is on sandwich structures with hexagonal core. Perfect bonding between core and facesheet, and between neighboring core walls is assumed. This implies that there are no delaminations or discontinuities present. Another assumption made in this study is that although the core walls are thin-walled structures, buckling under compression is disregarded.

The aim of this study is to present an analytical model accounting for skin-effect to allow the calculation of the stiffness of honeycomb cores as well as the interfacial stresses, both under in-plane and out-of-plane forces. Specifically, the objectives are:

1. Based on equilibrium conditions, derive a model that can accurately describe the displacement field for core walls.
2. Use this model to calculate stiffness and interfacial stresses, compare the results with existing and FE results, and define the skin effect on stiffness and interfacial stresses.
3. Carry out a parametric study on interfacial stresses, and identify the critical section in the structure where further consideration should be given for design purposes.

4. Out-of-plane shear behavior

4.1. Origin of shear warping

A honeycomb can be considered as an interconnected network of plates which form the faces of cells (Fig. 2). Following the definition by Grediac (1993), it can be characterized by four dimensionless aspect ratios:

$$R_1 = \frac{t}{b}, \quad R_2 = \frac{a}{b}, \quad R_3 = \frac{h}{a}, \quad R_4 = \frac{t'}{t} \tag{1}$$

where $h =$ height of core. It is assumed that the cell walls predominately carry load through membrane strains, and that the bending forces and bending effects in the cell walls can be neglected, which is consistent with a formulation for shear warping defined by Chen and Davalos (2004). All previous research is based on this assumption and it is also adopted here. Naturally, the thinner the core walls, the truer is this assumption.

The displacement field in cell walls can be described at two distinct regions: (1) at a position sufficiently faraway from the interface, such as at the mid-depth where the effect of rigid facesheet dissipates; this condition can be defined by force equilibrium; and (2) directly at the face–core interface by assuming that the facesheet is rigid, which is reasonable considering the stiffness ratio between the facesheet and core; in this case displacement compatibility is invoked, where strain transformation can be used to find the relationship between local and global strain. Therefore, the purpose of the analysis is to find a displacement field that can accurately describe these two distinct regions and the transition field in between.

4.1.1. Force equilibrium

Under a shear strain γ, the resulting distributed shear flow for a typical cell and its representative volume element (RVE) are shown in Figs. 3 and 4, respectively, where τ_1^f and τ_2^f are shear stresses acting respectively on the flat and inclined panel; the superscript f denotes *force* equilibrium. Due to the symmetry of the honeycomb, we can further reduce this cell into a model as shown in Fig. 5, which represents one quarter of one central wall and one quarter of one inclined wall.

Based on the model shown in Fig. 5, the equilibrium equations neglecting skin effect, i.e., considering the force equilibrium, can be written as (Gibson and Ashby, 1988)

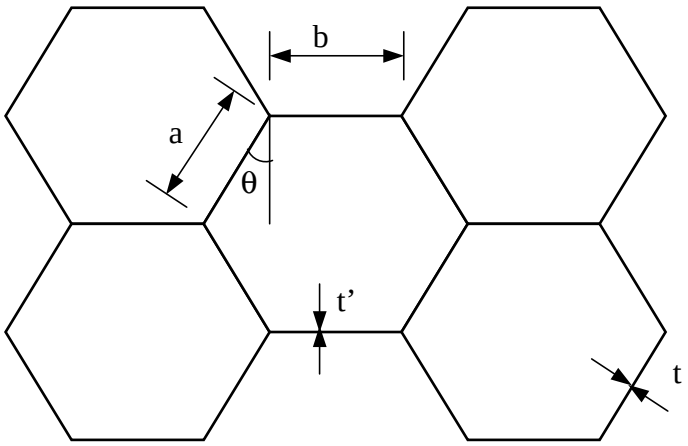

Fig. 2. Geometry of the honeycomb.

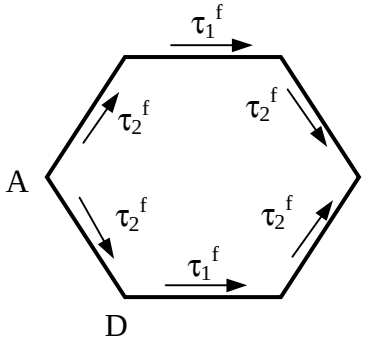

Fig. 3. Shear flow in the unit cell.

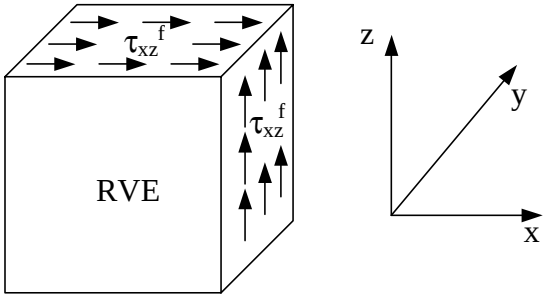

Fig. 4. Shear flow in the RVE.

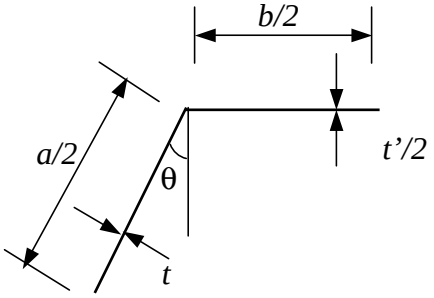

Fig. 5. Analysis model.

$$\tau_1^{\mathrm{f}} \frac{t'}{2} = \tau_2^{\mathrm{f}} t \tag{2}$$

$$\tau_{xz}^{\mathrm{f}} V = \tau_1^{\mathrm{f}} \frac{t'}{2} \frac{b}{2} + \tau_2^{\mathrm{f}} t \frac{a}{2} \sin\theta \tag{3}$$

where $V = \frac{1}{2}(b + a\sin\theta)a\cos\theta$; and a, b, t and t' are defined in Fig. 2. Solving for Eqs. (2) and (3), we have

$$\tau_1^{\mathrm{f}} = \frac{2R_2\cos\theta}{R_4 R_1} \tau_{xz}^{\mathrm{f}} \tag{4}$$

$$\tau_2^{\mathrm{f}} = \frac{R_2 \cos\theta}{R_1}\tau_{xz}^{\mathrm{f}} \tag{5}$$

The local shear strain can be obtained as

$$\gamma_1^{\mathrm{f}} = \frac{\tau_1^{\mathrm{f}}}{G} \qquad \gamma_2^{\mathrm{f}} = \frac{\tau_2^{\mathrm{f}}}{G} \tag{6}$$

where G is the shear modulus of the core material. The equivalent shear modulus G_{xz}^{f} can then be calculated as

$$\frac{1}{2}G_{xz}^{\mathrm{f}}(\gamma)^2 V = \sum_{i=1}^{2}\int_{V_i}\frac{1}{2}G(\gamma_i^{\mathrm{f}})^2\,\mathrm{d}V_i \tag{7}$$

where the summation represents the contribution of both panels. Using Eqs. (4)–(6) into Eq. (7), we obtain

$$G_{xz}^{\mathrm{f}} = \frac{(1+R_2\sin\theta)R_1}{\left(\frac{2}{R_4}+R_2\right)R_2\cos\theta}G \tag{8}$$

Correspondingly, we have

$$\tau_{xz}^{\mathrm{f}} = \gamma G_{xz}^{\mathrm{f}} \tag{9}$$

Based on Eq. (6)–(9), the local–global strain relationships due to force equilibrium can be written as

$$\gamma_1^{\mathrm{f}} = \frac{2(1+R_2\sin\theta)}{(2+R_2R_4)}\gamma \tag{10}$$

$$\gamma_2^{\mathrm{f}} = \frac{1+R_2\sin\theta}{\left(\frac{2}{R_4}+R_2\right)}\gamma \tag{11}$$

where γ_1^{f} and γ_2^{f} are local shear strains in the flat and inclined panel, respectively, due to force equilibrium. It is implied that both the flat panel and inclined panel will deform in a straight line, as shown in Fig. 6.

4.1.2. Displacement compatibility

At the face–core interface, the rigid skin strains enforce the following cell wall deflection or strain transformation

$$\gamma_1^{\mathrm{d}} = \gamma \tag{12}$$

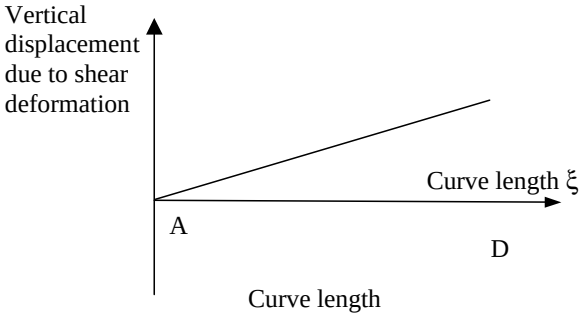

Fig. 6. Assumed deformed shape.

$$\gamma_2^{\mathrm{d}} = \gamma \sin\theta \tag{13}$$

where γ_1^{d} and γ_2^{d} are local shear strains in the flat and inclined panel, respectively, due to displacement compatibility, as denoted by the superscript d. Once again, the panels are assumed to deform in a straight line.

4.1.3. Deformation incompatibility

From the discussion above, we can observe that, although the flat and inclined panel will deform in a straight line under both force equilibrium and displacement compatibility conditions, a deformation incompatibility results due to the different strain states. This phenomenon can be described through two steps. In the first step, the core wall will deform in a way without considering skin effect, where uniform stress and strain distribution can be assumed, which implies that the upper and lower faces of the core elements are not constrained in the transverse direction. However, due to the presence of the relatively rigid facesheets, the core is forced to deform consistently with the skins. Thus, in the second step, due to the deformation incompatibility, the shear warping will be present at the top and bottom of the flat and inclined panels, which can be defined as a boundary condition. The formulation can be simplified as a plane-stress problem subject to a shear strain with the following boundary condition caused by the deformation incompatibility

$$\varphi_i(\xi) = (\gamma_i^{\mathrm{d}} - \gamma_i^{\mathrm{f}})\xi \tag{14}$$

where ξ is the local coordinate along the panel, $i = 1, 2$ correspond to the flat and inclined panel, respectively. The final strain state is therefore the summation of the strains obtained for the above two steps.

4.2. Theoretical analysis

Penzien and Didriksson (1964) firstly presented a solution for this problem. However, they assumed the plate is rigid along the ξ direction and the component of σ_ξ is thereby neglected, which is not reasonable. A refined derivation is therefore presented as follows. It is noted that the derivation is applicable for both flat and inclined panels, and therefore, the subscript i is omitted for simplicity.

Consider the element ABCD in Fig. 7, which is cut from the unit cell shown in Fig. 3, subject to a shear strain γ. The equilibrium equations for the stresses acting on the $\xi\eta$ plane in the absence of body forces are

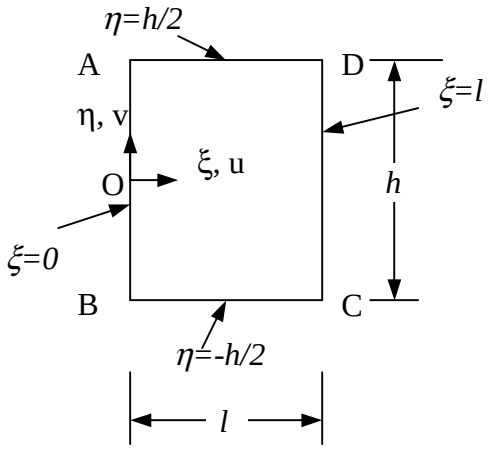

Fig. 7. Model cut from the structure.

$$\frac{\partial \sigma_\xi}{\partial \xi} + \frac{\partial \tau_{\xi\eta}}{\partial \eta} = 0 \tag{15a}$$

$$\frac{\partial \tau_{\xi\eta}}{\partial \xi} + \frac{\partial \sigma_\eta}{\partial \eta} = 0 \tag{15b}$$

The stress–strain relationships are

$$\begin{Bmatrix} \sigma_\xi \\ \sigma_\eta \\ \tau_{\xi\eta} \end{Bmatrix} = \begin{bmatrix} E' & vE' & 0 \\ vE' & E' & 0 \\ 0 & 0 & G \end{bmatrix} \begin{Bmatrix} \varepsilon_\xi \\ \varepsilon_\eta \\ \gamma_{\xi\eta} \end{Bmatrix} \tag{16}$$

where, $E' = \frac{E}{1-v^2}$, $G = \frac{E}{2(1+v)}$, $E =$ Young's modulus, and $v =$ Poisson's ratio. The strain–displacement relations are

$$\varepsilon_\xi = \frac{\partial u}{\partial \xi} \tag{17a}$$

$$\varepsilon_\eta = \frac{\partial v}{\partial \eta} \tag{17b}$$

$$\gamma_{\xi\eta} = \frac{\partial u}{\partial \eta} + \frac{\partial v}{\partial \xi} \tag{17c}$$

where u and v are the displacement in the ξ and η directions, respectively. For the consideration of shear warping, we can assume that there is no stretching in the ξ direction. Then we have

$$u = u(\eta) \qquad \varepsilon_\xi = 0 \tag{18}$$

Eq. (16) can then be reduced to

$$\sigma_\xi = vE'\varepsilon_\eta \tag{19a}$$

$$\sigma_\eta = E'\varepsilon_\eta \tag{19b}$$

$$\tau_{\xi\eta} = G\gamma_{\xi\eta} \tag{19c}$$

Differentiating Eqs. (19b) and (19c) with respect to η and ξ, respectively, substituting into Eq. (15b), and using Eqs. (17b) and (17c), one obtains

$$G\frac{\partial^2 v}{\partial \xi^2} + E'\frac{\partial^2 v}{\partial \eta^2} = 0 \tag{20}$$

From the boundary conditions shown in Fig. 7, $u(\eta) = 0$ at both $\eta = h/2$ and $\eta = -h/2$, and therefore u is negligible throughout the panel. Then, Eq. (19) becomes

$$\sigma_\xi = vE'(\partial v/\partial \eta) \tag{21a}$$

$$\sigma_\eta = E'(\partial v/\partial \eta) \tag{21b}$$

$$\tau_{\xi\eta} = G(\partial v/\partial \xi) \tag{21c}$$

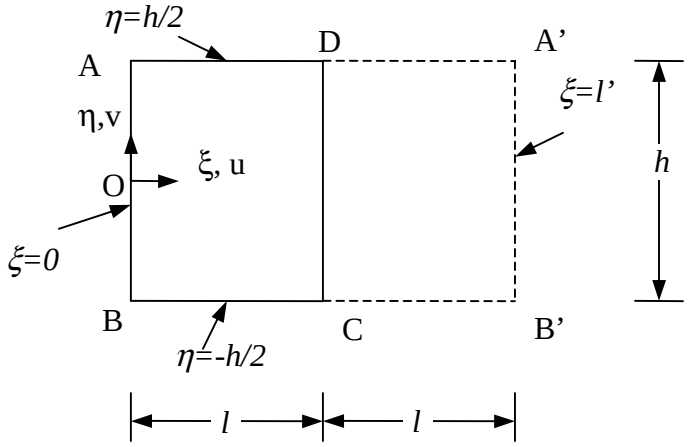

Fig. 8. Theoretical model.

Eqs. (20) and (21) act as the basis for this analytical study. In order to use Fourier series to solve Eq. (20), appropriate boundary conditions should be considered. To do this, we can add a fictitious plate DCB'A', as the mirror image of ABCD, about line CD, with a symmetric displacement field, as shown in Fig. 8. The boundary conditions can be described as:

$$v(0,\eta) = v(l',\eta) = 0 \tag{22a}$$

$$v(\xi,\eta) = v(\xi,-\eta) \tag{22b}$$

$$v(\xi,h/2) = \begin{cases} \varphi(\xi) & \text{if } \xi \leqslant l \\ \varphi'(\xi) & \text{if } l < \xi \leqslant l' \end{cases} \tag{22c}$$

where l is the panel length, h is the height, and $l' = 2l$. The function $\varphi(\xi)$, caused by shear warping, is defined in Eq. (14), and based on symmetry, $\varphi'(\xi)$ can be similarly defined as

$$\varphi_i'(\xi) = (\gamma_i^{\mathrm{d}} - \gamma_i^{\mathrm{f}})(l' - \xi) \tag{23}$$

The functions $\varphi(\xi)$ and $\varphi'(\xi)$ are illustrated in Fig. 9.

The solution of the partial differential Eq. (20) with boundary conditions (22) can be obtained by using Fourier series. Thus, through some simple mathematical transformations, the transverse displacement can be described as

$$v(\xi,\eta) = \sum_{n=1}^{\infty} \left[\frac{2/l'}{\cosh\left(\frac{n\pi h}{2l'\mu}\right)} \varphi_n \cosh\left(\frac{n\pi\eta}{l'\mu}\right) \sin\left(\frac{n\pi\xi}{l'}\right) \right] \tag{24}$$

where

$$\mu = \sqrt{E'/G} \tag{25}$$

$$\varphi_n = \int_0^l \varphi(\xi) \sin\frac{n\pi\xi}{l'} \mathrm{d}\xi + \int_l^{l'} \varphi'(\xi) \sin\frac{n\pi\xi}{l'} \mathrm{d}\xi \tag{26}$$

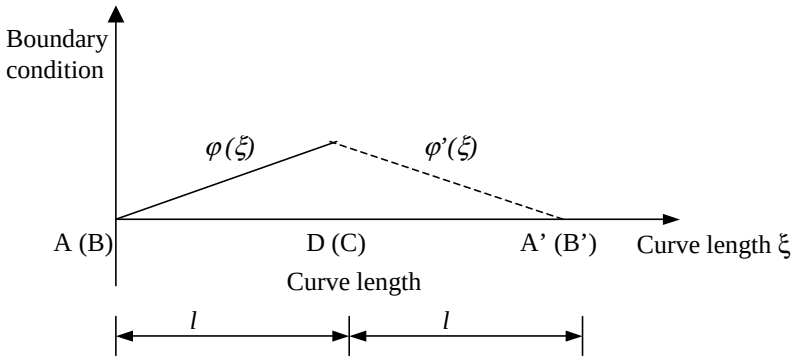

Fig. 9. Boundary conditions.

The normal stress σ_η can be obtained using Eq. (19b) as

$$\sigma_\eta(\xi,\eta) = E'(\partial v/\partial\eta) = \sum_{n=1}^{\infty}\left[\frac{2n\pi}{l'^2\mu\cosh\left(\frac{n\pi h}{2l'\mu}\right)}\varphi_n \sinh\left(\frac{n\pi\eta}{l'\mu}\right)\sin\left(\frac{n\pi\xi}{l'}\right)\right] \tag{27}$$

Eq. (19c) gives

$$\tau_{\xi\eta}(\xi,\eta) = G(\partial v/\partial\xi) = \sum_{n=1}^{\infty}\left[\frac{2n\pi}{l'^2\cosh\left(\frac{n\pi h}{2l'\mu}\right)}\varphi_n \sinh\left(\frac{n\pi\eta}{l'\mu}\right)\cos\left(\frac{n\pi\xi}{l'}\right)\right] \tag{28}$$

The total shear stress can then be calculated as

$$\tau_i(\xi,\eta) = \tau_i^{\mathrm{f}}(\xi,\eta) + \tau_{\xi\eta i}(\xi,\eta) \tag{29}$$

The normal stress σ_ξ can be obtained using Eq. (19a).

Next, the total strain energy is defined as

$$U = \sum\int\frac{[\tau_i(\xi,\eta)]^2}{2G}dV + \sum\int\frac{[\sigma_{\eta i}(\xi,\eta)]^2}{2E'}\,\mathrm{d}V \tag{30}$$

in order to calculate the equivalent shear modulus G_e as

$$G_e = \frac{2U}{V\gamma^2} \tag{31}$$

where U is the total strain energy, V is the volume corresponding to the RVE, γ is the shear strain applied to the structure. The above equations can be incorporated into any mathematical software such as MATHCAD.

4.3. Verification

4.3.1. Stiffness

Grediac (1993) carried out a comprehensive study on the stiffness of hexagonal honeycomb core using FE and considering skin effect. In his study, $R_1 = 0.08$, $R_2 = 1$, and R_3 is varied between 1 and 10. The material properties are $E = 72\,\mathrm{GPa}$ and $\nu = 0.31$. Four cell geometries were studied: $\theta = 0°$, 10°, 20° and 30°. These results are reproduced in the present study for verification purposes. Figs. 10–13 show the shear

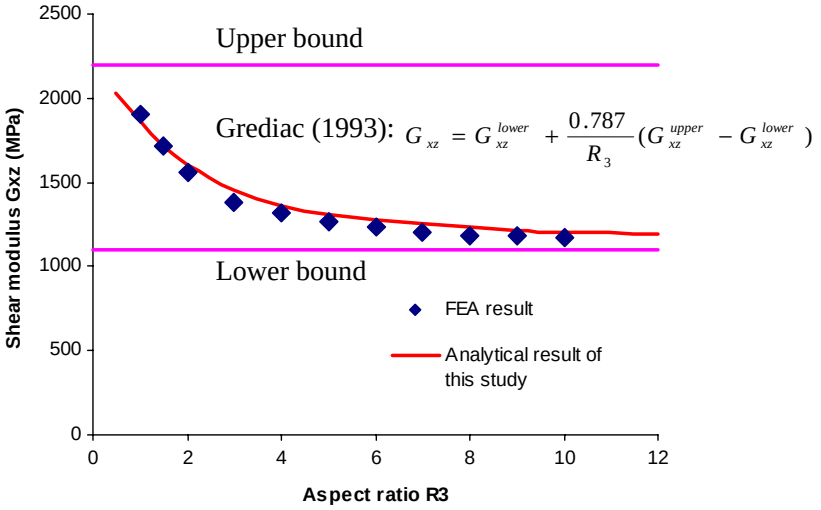

Fig. 10. Shear modulus G_{xz} vs. aspect ratio R_3, $\theta = 0°$.

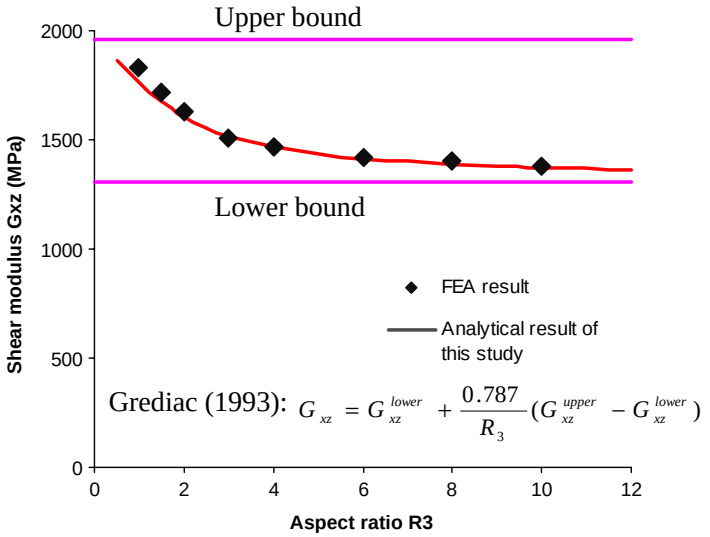

Fig. 11. Shear modulus G_{xz} vs. aspect ratio R_3, $\theta = 10°$.

modulus G_{xz} vs. aspect ratio R_3 curves from FE and the present analytical solution, where we can see that there is a good correlation between the two results, which corroborate the accuracy of the analytical model derived herein. The upper and lower bounds, and the empirical formulas given in these figures were provided by Grediac (1993).

4.3.2. Stress distribution

Since there is no study available on the interfacial stresses, FE is further employed to calculate the interfacial stress distribution. A partial unit cell of an hexagonal honeycomb sandwich core geometry is shown

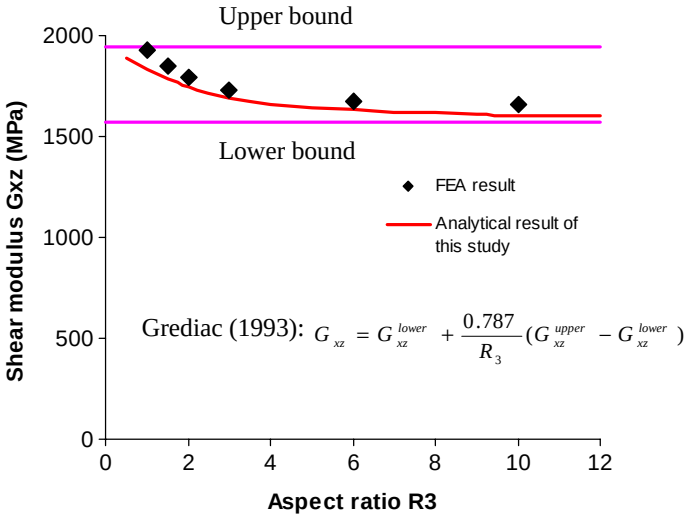

Fig. 12. Shear modulus G_{xz} vs. aspect ratio R_3, $\theta = 20°$.

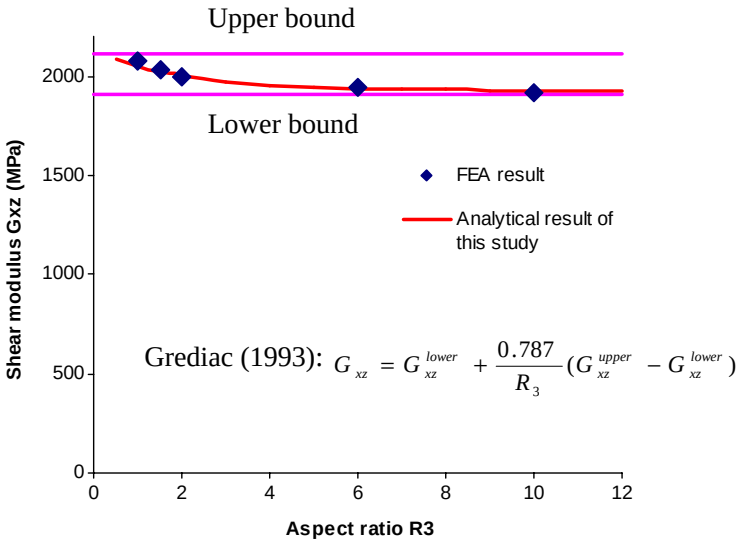

Fig. 13. Shear modulus G_{xz} vs. aspect ratio R_3, $\theta = 30°$.

in Fig. 5. Due to the symmetric structure, we can model a quarter-cell, as shown in Fig. 14, where the thickness is $t'/2$ for the flat panels and t for the inclined panel. The dimensions and properties of the core materials are listed in Table 1. ABAQUS (2001) is adopted for the FE analysis. The core walls are modelled with a four-node shell element, S4, and the model consists of 800 elements. Through a convergence study, this mesh provided sufficiently accurate results for this study.

In the FE analysis, all the nodes at the top face translate at a uniform displacement in the x-direction. Thus, the shear and normal stress distributions can be obtained. The boundary conditions are listed in Table 2, which are the same as those used by Grediac (1993). Fig. 15 shows the stress distributions along

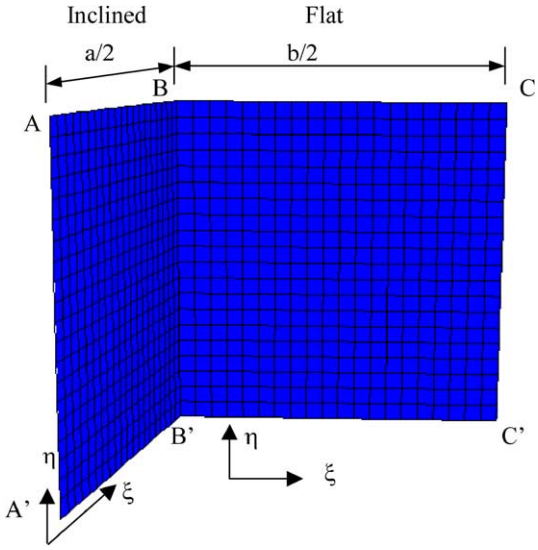

Fig. 14. FE model.

Table 1
Dimensions and properties of core material

a (mm)	b (mm)	h (mm)	t (mm)	t' (mm)	θ (°)	E (MPa)	v
1	1	2	0.08	0.08	10	72000	0.31

Table 2
Boundary conditions of FE model

	u	v	w
AA′	Free	Free	0
CC′	Free	0	0
AB/BC	Constant	0	0
A′B′/B′C′	0	0	Free

the top of the inclined and flat panels, as calculated both from analytical and FE results. The local contour coordinate, ξ, is directed from A to B (or 0–0.5 mm) for the inclined panel, and from B to C (or 0.5–1.0 mm) for the flat panel. A good correlation can be observed from the comparisons, although there are some discrepancies for the shear stress due to some limiting assumptions adopted in this study. These favorable comparisons illustrate the accuracy of the analytical method for predicting the behavior of the panels under shear warping.

It is interesting to observe that at the intersection of inclined and flat panel, a significant normal stress σ_η either in compression or tension, depending on the shear force direction, arises due to the shear strain induced, making this intersection a critical location in design. This stress drops rapidly at locations away from the intersection, and reaches zero at the mid-span of both flat and inclined panels. The shear stress in the flat panel is much higher than that in the inclined panel, indicating that the flat panel carries most of the shear force. A contour plot of σ_η from FE is given in Fig. 16, where we can see that the stress at

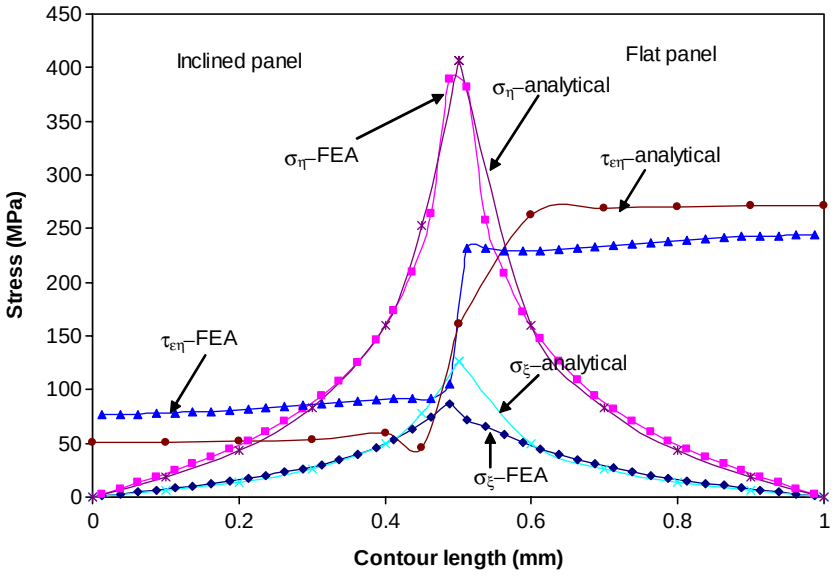

Fig. 15. Interfacial stress distribution.

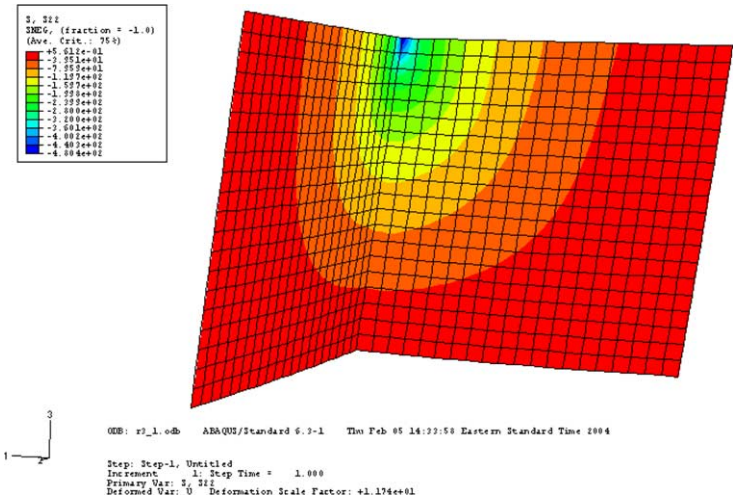

Fig. 16. Contour plot for normal stress σ_η.

the panel-intersection is higher around the core–skin interface, and reaches nearly zero at the mid-height of the core. This illustrates the stress concentration effect that the skin induces on the core at the interface.

4.4. Application

Using the closed-form solution derived in this chapter, a parametric study is carried out for the interfacial normal stress, σ_η, at the panel intersection, as shown in Fig. 17. From which, we can observe that σ_η

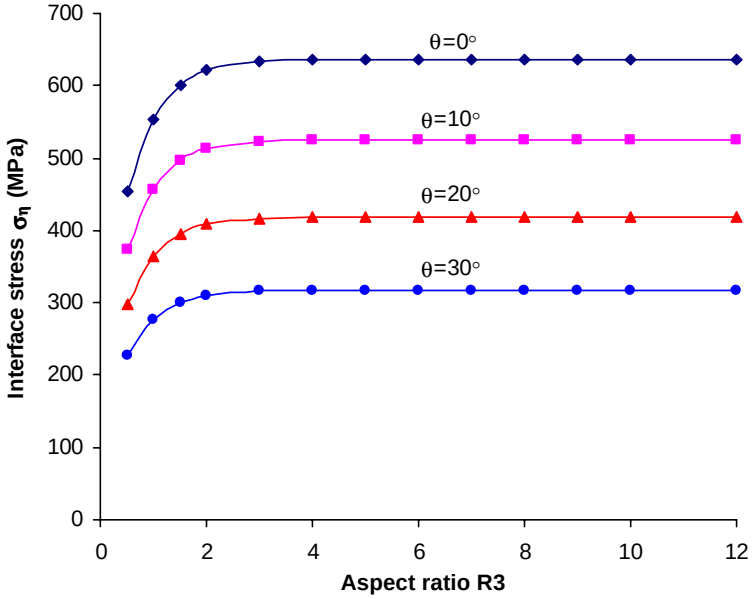

Fig. 17. Parametric study on interfacial stress.

increases as the aspect ratio increases, and reaches a constant value beyond a certain limit, for instance, $R_3 \approx 2$ for this case. For $\theta = 0°$ case, which corresponds to a rectangular shape, σ_η is a maximum. As θ increases, the interfacial stress decreases. It is expected that when $\theta = 90°$ i.e., no inclined panel exists in the core configurations, σ_η will vanish since no warping will occur.

4.5. Summary and discussion for out-of-plane shear

An analytical solution for a general hexagonal core including skin-effect and subjected to transverse shear is presented in this section. From the above results, we can conclude:

1. The present analytical solution can successfully predict the behavior of honeycomb cores accounting for shear warping, both in terms of stiffness and interfacial stresses, which are verified by FE results.
2. The shear modulus can be accurately obtained from this model, minimizing the error caused by neglecting the skin effect. The solution is explicit and easy to implement.
3. The skin effect is a localized phenomenon. The lower bound of the equivalent stiffness can thereby be adopted if the aspect ratio is high enough. However, the skin-effect can significantly affect interfacial stress distribution, yielding a coupled stress state, where the normal stress may even be larger than the shear stress. This indicates that, unlike the common belief that only shear stress occurs when the structure is under pure shear force, tension force at the interface arises for a sandwich core, especially at the intersections of core elements, making such locations critical in design. Therefore, special considerations are necessary in design applications.
4. The skin effect described herein affects the stress distribution of both the flat and inclined panel. This effect on the stress distribution becomes less significant in the area away from the interface.
5. The results provided in this study, together with interfacial shear and flatwise tension test results, can be used for failure predictions of honeycomb sandwich panels.

5. In-plane behavior

Unlike the attention that out-of-plane shear has received, there is limited information available on in-plane behavior, and the only possible work considering skin effect was published by Becker (1998), who provided a closed-form solution for in-plane moduli and used FE analysis for verification of results. We note, however, that the displacement function he assumed is empirical and most likely not applicable for prediction of interfacial stresses. Also, Becker's solution is implicit and difficult to implement. Therefore, it is the aim of this study to provide an explicit solution for in-plane behavior, which can not only predict stiffness but also interfacial stresses.

5.1. In-plane stretch

As discussed in Section 4, there are two distinct displacement fields for a sandwich core when considering skin effect: force equilibrium at the mid-depth and displacement compatibility at the interface. The expressions for these two fields are given as follows.

5.1.1. Force equilibrium

Strain state subjected to ε_x^0

When a uniform strain of ε_x^0 is applied to the structure, as shown in Fig. 18, axial forces F_1 and F_2 in the flat and inclined panel result. When a unit height is considered, it is found that

$$F_1 = F_2 \sin\theta \tag{32}$$

$$\sigma_1^{\mathrm{f}} = \frac{F_1}{t'/2} \qquad \sigma_2^{\mathrm{f}} = \frac{F_2}{t} \tag{33}$$

where σ_1^{f} and σ_2^{f} are axial stresses due to force equilibrium in the flat and inclined panel, respectively.

The strain energy can be written as

$$U = \sum \int \frac{(\sigma_i^{\mathrm{f}})^2}{2E}\,\mathrm{d}A = F_1^2\left(\frac{b}{2Et'} + \frac{a}{4Et\sin^2\theta}\right) \tag{34}$$

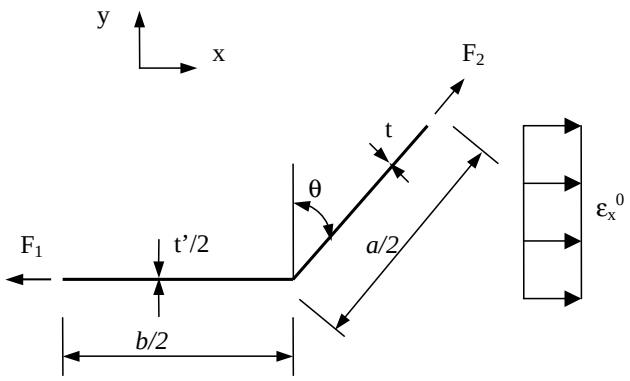

Fig. 18. Model subjected to ε_x^0.

The apparent strain value in the flat panel, ε_1^f, can be calculated through Castigliano's second theorem. The theorem states that under the principal of superstition, a partial derivative of the strain energy with respect to an external force gives the displacement corresponding to that force. In this case, the displacement in the x-direction can be obtained as

$$\frac{\partial U}{\partial F_1} = \frac{1}{2}(b + a\sin\theta)\varepsilon_x^0 \tag{35}$$

Substituting Eq. (34) into Eq. (35), we have

$$\frac{\partial U}{\partial F_1} = F_1\left(\frac{b}{Et'} + \frac{a}{2Et\sin^2\theta}\right) = \varepsilon_1^f\left(\frac{b}{2} + \frac{aR_4/2}{2\sin^2\theta}\right) \tag{36}$$

Solving for Eqs. (35) and (36), the local–global strain relationship can be described as

$$\varepsilon_1^f = \varepsilon_x^0 \frac{\sin^2\theta(b + a\sin\theta)}{b\sin^2\theta + aR_4/2} \tag{37}$$

$$\varepsilon_2^f = \varepsilon_x^0 \frac{\sin\theta(b + a\sin\theta)R_4/2}{b\sin^2\theta + aR_4/2} \tag{38}$$

For a particular case, when $a = b$, $\theta = 30^\circ$ and $R_4 = 2$, the results reduce to

$$\varepsilon_1^f = \frac{3}{10}\varepsilon_x^0 \quad \varepsilon_2^f = \frac{3}{5}\varepsilon_x^0 \tag{39}$$

Strain state subjected to ε_y^0

Similarly, we can apply a uniform strain ε_y^0 in the y-direction, as shown in Fig. 19. The force F_2 can be decomposed into F_v and F_h. The component F_v can be written as

$$F_v = F_2\cos\theta = F_1\tan\theta \tag{40}$$

Following the same approach as above, we can obtain

$$\frac{\partial U}{\partial F_v} = \frac{F_1}{\tan\theta}\left(\frac{b}{Et'} + \frac{a}{2Et\sin^2\theta}\right) = \varepsilon_1^f\frac{1}{\tan\theta}\left(\frac{b}{2} + \frac{aR_4/2}{2\sin^2\theta}\right) \tag{41}$$

$$\frac{\partial U}{\partial F_v} = \frac{a}{2}\cos\theta\varepsilon_y^0 \tag{42}$$

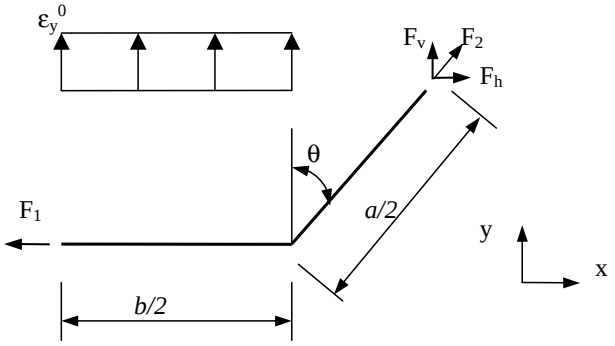

Fig. 19. Model subjected to ε_y^0.

Solving for Eqs. (41) and (42), we have

$$\varepsilon_1^{\mathrm{f}} = \varepsilon_y^0 \frac{a\sin^3\theta}{b\sin^2\theta + aR_4/2} \tag{43a}$$

$$\varepsilon_2^{\mathrm{f}} = \varepsilon_y^0 \frac{a\sin^2\theta R_4/2}{b\sin^2\theta + aR_4/2} \tag{43b}$$

For a particular case, when $a = b$, $\theta = 30°$, and $R_4 = 2$, the results become

$$\varepsilon_1^{\mathrm{f}} = \frac{1}{10}\varepsilon_y^0 \quad \varepsilon_2^{\mathrm{f}} = \frac{1}{5}\varepsilon_y^0 \tag{44}$$

5.1.2. Displacement compatibility

At the interface, when the facesheet is assumed to be rigid, the strain state can be obtained through strain transformation as

$$\varepsilon_1^{\mathrm{d}} = \varepsilon_x^0 \tag{45a}$$

$$\varepsilon_2^{\mathrm{d}} = \sin^2\theta\varepsilon_x^0 + \cos^2\theta\varepsilon_y^0 \tag{45b}$$

5.1.3. Deformation incompatibility

An apparent strain incompatibility arises from the two displacement fields, which can be described as

$$\Delta\varepsilon_i = \varepsilon_i^{\mathrm{f}} - \varepsilon_i^{\mathrm{d}} \tag{46}$$

where $i = 1,2$ correspond to the flat panel and inclined panel, respectively.

5.2. Theoretical analysis

From the discussion in Section 5.1, we conclude that there are two distinct strain fields at the interface and the mid-depth. This problem can be approached through two steps: firstly, the core wall is permitted to freely move with stress q_1 acting at the free edge (Fig. 20), resulting in a uniform strain state in the whole plate, with the magnitude equal to the strain at interface $\varepsilon_i^{\mathrm{d}}$. From basic assumptions, we have

$$q_1 = E'\varepsilon_i^{\mathrm{d}} \tag{47}$$

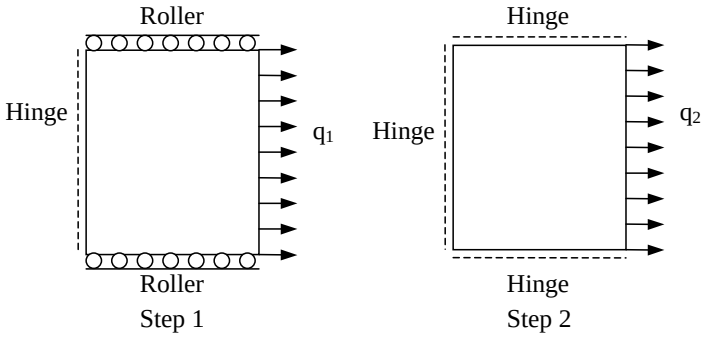

Fig. 20. Two-step simulation. Step1: Uniform stretch. Step 2: Additional strain.

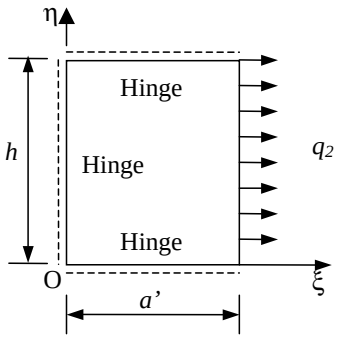

Fig. 21. Theoretical model.

Secondly, q_2 is applied at the free edge with three sides simply supported to induce additional strain, as shown in Fig. 20. The stress q_2 can be expressed as

$$q_2 = E'\Delta\varepsilon_i \tag{48}$$

The final strain state is the summation of the strains from these two steps. The solution for the first step can be easily obtained, whereas for step two, the solution requires further consideration; one approach is to treat the problem as a plate with three sides simply supported under a uniform stress at the free edge, leading to an explicit solution as given next.

The analytical model is shown in Fig. 21. The dimension $a' = b/2$ and $a/2$ for the flat and inclined panel, respectively. Following the derivation in Section 4, when the displacement v is neglected for a plane-stress problem, the governing equation is written as

$$E'\frac{\partial^2 u}{\partial \xi^2} + G\frac{\partial^2 u}{\partial \eta^2} = 0 \tag{49}$$

As described in Section 4.2, the solution of the partial differential Eq. (49) can be obtained by using Fourier series, defined as

$$u(\xi,\eta) = \sum_{n=1}^{\infty}\left[C_n \cosh\left(\frac{n\pi\xi}{h\mu}\right) + D_n \sinh\left(\frac{n\pi\xi}{h\mu}\right)\right]\sin\left(\frac{n\pi\eta}{h}\right) \tag{50}$$

with the boundary conditions:

$$u(\xi,0) = u(\xi,h) = 0$$

$$u(0,\eta) = 0 \tag{51}$$

Substituting the boundary conditions into Eq. (50), we find $C_n = 0$. Then Eq. (50) can be simplified to be

$$u(\xi,\eta) = \sum_{n=1}^{\infty} D_n \sinh\left(\frac{n\pi\xi}{h\mu}\right)\sin\left(\frac{n\pi\eta}{h}\right) = \sum_{n=1}^{\infty} D_n f_1(n,\xi,\eta) \tag{52}$$

Then, in a similar manner as shown in Section 4, we obtain the strains as

$$\varepsilon_\xi(\xi,\eta) = \frac{\partial u}{\partial \xi} = \sum_{n=1}^{\infty} D_n \frac{n\pi}{h\mu}\cosh\left(\frac{n\pi\xi}{h\mu}\right)\sin\left(\frac{n\pi\eta}{h}\right) = \sum_{n=1}^{\infty} D_n f_2(n,\xi,\eta) \tag{53}$$

$$\gamma_{\xi\eta}(\xi,\eta)=\frac{\partial u}{\partial \eta}=\sum_{n=1}^{\infty}D_n\frac{n\pi}{h}\sinh\left(\frac{n\pi\xi}{h\mu}\right)\cos\left(\frac{n\pi\eta}{h}\right)=\sum_{n=1}^{\infty}D_n f_3(n,\xi,\eta) \tag{54}$$

Next, we use energy concepts to obtain effective stiffnesses and interfacial stresses. The total potential energy is

$$\Pi=U+W \tag{55}$$

where

$$U=\int\int\left[\frac{1}{2}E'\varepsilon_{\xi}^2(\xi,\eta)+\frac{1}{2}G\gamma_{\xi\eta}^2(\xi,\eta)\right]\mathrm{d}\xi\,\mathrm{d}\eta \tag{56}$$

and

$$W=-\int_0^h q_2 u(a',\eta)\,\mathrm{d}\eta \tag{57}$$

The first variation of Π, leads to necessary condition for equilibrium, or minimum potential energy, as

$$\delta\Pi=\delta U+\delta W=0 \tag{58}$$

We can define the following displacement and strain gradients in terms of parameters $D_1, D_2, \ldots, D_m$:

$$\frac{\partial u(\xi,\eta)}{\partial D_m}=f_1(m,\xi,\eta) \tag{59a}$$

$$\frac{\partial \varepsilon_{\xi}(\xi,\eta)}{\partial D_m}=f_2(m,\xi,\eta) \tag{59b}$$

$$\frac{\partial \gamma_{\xi\eta}(\xi,\eta)}{\partial D_m}=f_3(m,\xi,\eta) \tag{59c}$$

Then, substituting Eqs. (59b) and (59c) into the first variation of Eq. (56), we have

$$\delta U=\left(\int\int\left[E'\varepsilon_{\xi}(\xi,\eta)f_2(m,\xi,\eta)+G\gamma_{\xi\eta}(\xi,\eta)f_3(m,\xi,\eta)\right]\mathrm{d}\xi\,\mathrm{d}\eta\right)\delta D_m \tag{60}$$

Similarly, substituting Eq. (59a) into the first variation of Eq. (57), we have

$$\delta W=\left[-\int_0^h q_2 f_1(m,a',\eta)\,\mathrm{d}\eta\right]\delta D_m \tag{61}$$

Further, it can be shown that

$$int_0^h \sin\frac{m\pi\eta}{h}\sin\frac{n\pi\eta}{h}\,\mathrm{d}\eta=\frac{h}{2}\delta_{mn} \tag{62}$$

where δ_{mn} is the Kronecker delta defined as

$$\delta_{mn}=\begin{cases}1 & \text{if } m=n\\ 0 & \text{if } m\neq n\end{cases} \tag{63}$$

Then Eq. (60) becomes

$$\delta U=\left[\frac{E'h\alpha^2(m)}{2}\int_0^{a'}\cosh^2(\alpha(m)\xi)\,\mathrm{d}\xi+\frac{Gh\mu^2\alpha^2(m)}{2}\int_0^{a'}\sinh^2(\alpha(m)\xi)\,\mathrm{d}\xi\right]D_m\delta D_m \tag{64}$$

where

$$\alpha(m) = \frac{m\pi}{h\mu} \tag{65}$$

Finally, substituting Eqs. (61) and (64) into Eq. (58), and considering δD_m is an arbitrary value, D_m is defined as

$$D_m = \frac{[1-\cos(m\pi)]q_2 \sin[a'\alpha(m)]}{\frac{h\mu z^3(m)}{2}\left[E'\left(\frac{\sinh(2a'\alpha(m))}{4\alpha(m)}+\frac{a'}{2}\right)+\mu^2 G\left(\frac{\sinh(2a'\alpha(m))}{4\alpha(m)}-\frac{a'}{2}\right)\right]} = \psi(m,a',h)q_2 \tag{66}$$

It is noted that D_m is only related to the uniform stress q_2, that is, an explicit solution is given for D_m. Now, introducing D_m into Eq. (52)–(54), the expressions for the displacement, normal strain and shear strain can be obtained.

Next, we use the total strain energy, and corresponding strain energy density, to finally define the effective stiffnesses and corresponding stresses. The total normal strain is

$$\varepsilon_i(\xi,\eta) = \varepsilon_i^{\mathrm{d}} + \varepsilon_{\xi i}(\xi,\eta) \tag{67}$$

The total strain energy U is defined as

$$U = \sum \int\int \left[\frac{1}{2}E'(\varepsilon_i(\xi,\eta))^2 + \frac{1}{2}G(\gamma_{\xi\eta i}(\xi,\eta))^2\right] \mathrm{d}\xi\,\mathrm{d}\eta \tag{68}$$

with the strain energy density given as

$$U^* = \frac{U}{V} \tag{69}$$

Thus, the effective stiffnesses can be defined as

$$E_{xx} = \frac{\partial^2 U^*}{\partial \varepsilon_x^{02}} \tag{70a}$$

$$E_{yy} = \frac{\partial^2 U^*}{\partial \varepsilon_y^{02}} \tag{70b}$$

$$E_{xy} = \frac{\partial^2 U^*}{\partial \varepsilon_x^0 \partial \varepsilon_y^0} \tag{70c}$$

These effective stiffnesses correspond to homogenized unit cell stress (total force per cross sectional area A), in terms of macroscopic strains, as follows

$$\begin{Bmatrix} \sigma_x \\ \sigma_y \end{Bmatrix} = \begin{bmatrix} E_{xx} & E_{xy} \\ E_{xy} & E_{yy} \end{bmatrix} \begin{Bmatrix} \varepsilon_x^0 \\ \varepsilon_y^0 \end{Bmatrix} \tag{71}$$

5.3. Verification

5.3.1. Stiffness

For verification purpose, the derived explicit closed-form solution is used to solve the same problem studied by Becker (1998), where $a = b = 4\,\mathrm{mm}$, $t = t' = 0.05\,\mathrm{mm}$, $\theta = 30°$, and a set of core thickness h is varied. The cell wall material is aluminum with Young's Modulus $E = 72.2\,\mathrm{GPa}$ and Poisson's ratio $v = 0.34$. A finite element mesh of the representative unit cell is shown in Fig. 22. The stiffness vs. aspect

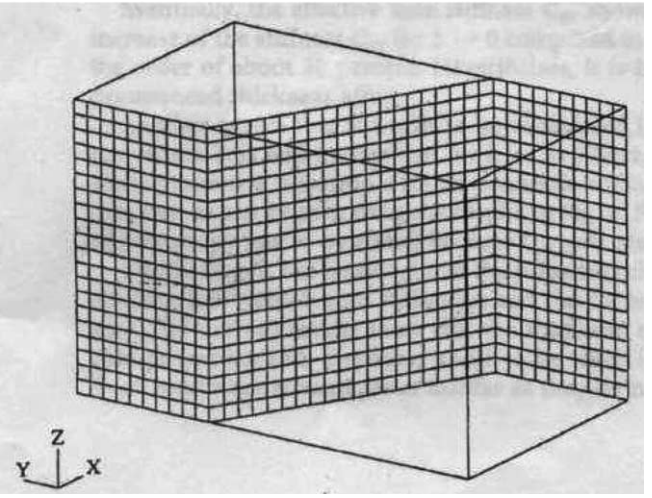

Fig. 22. Finite element mesh from Becker (1998).

ratio curves calculated from Becker's solution, the present closed-form solution and FE are shown in Fig. 23, where the discrete markers represent the FE results obtained from Becker (1998). Good correlations between the present analytical results and FE results can be observed, which shows the accuracy of the closed-form solution presented in this study. It should be noted that although different displacement functions are adopted in Becker's solution and in the present study, the difference between the two results for the stiffness is not significant. This is because the stiffness is a global property, and it is not affected much by the

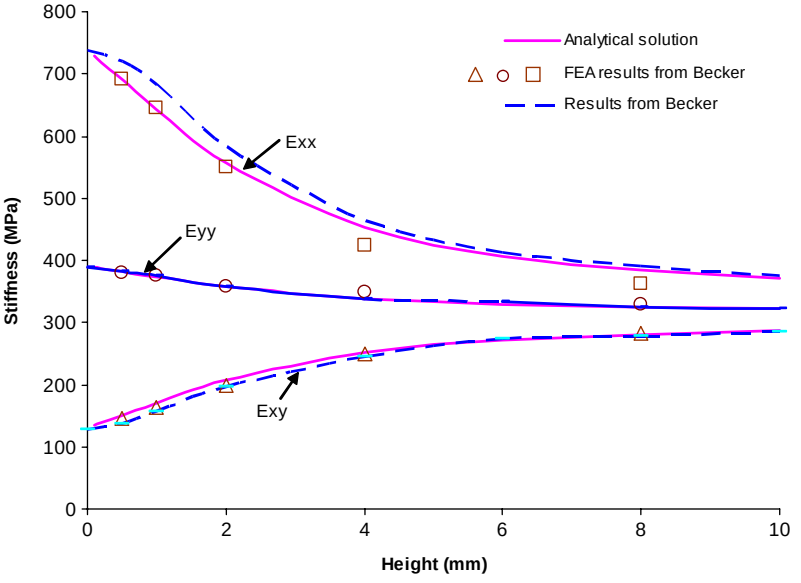

Fig. 23. Stiffness vs. height.

form of the displacement function. However, it is argued that the stress distribution is greatly affected by the choice of displacement function. The accuracy of the present solution for predicting stresses is illustrated next.

5.3.2. Stress distribution

To further validate the closed-form solution obtained, FE method and the analytical solution are both employed to study the interfacial stresses for $h = 4\,\text{mm}$. Exploiting symmetry, the FE model with contour plots of displacement u under $\varepsilon_x^0 = 0.01$ is shown in Fig. 24, where the skins are also included. A contour plot of shear stress is given in Fig. 25. Figs. 26–29 show the shear and normal stresses vs. distance under

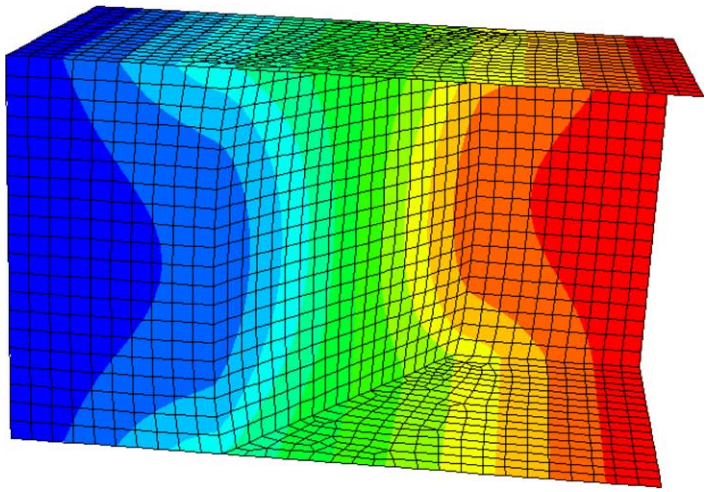

Fig. 24. FE model with contour plot for displacement u subjected to $\varepsilon_x^0 = 0.01$.

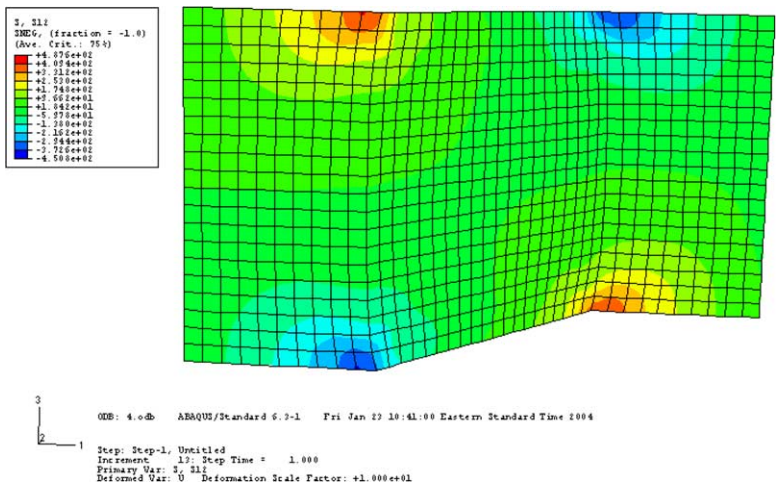

Fig. 25. Contour plot for $\sigma_{\xi\eta}$ subjected to $\varepsilon_x^0 = 0.01$.

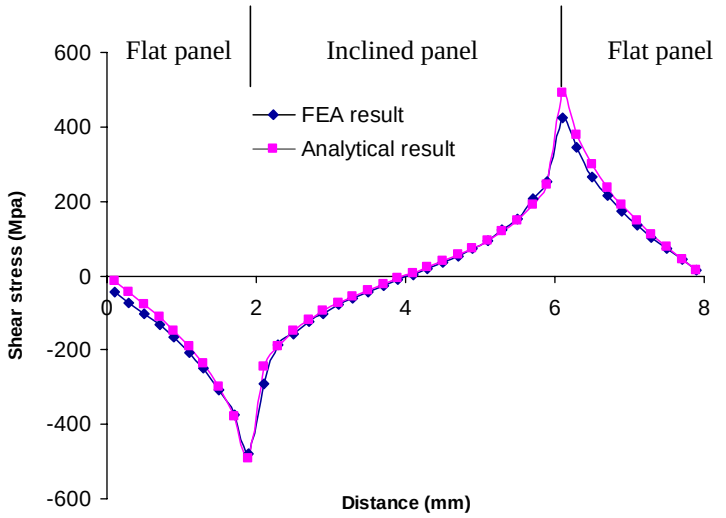

Fig. 26. Interfacial shear stress distribution: $\varepsilon_x^0 = 0.01$.

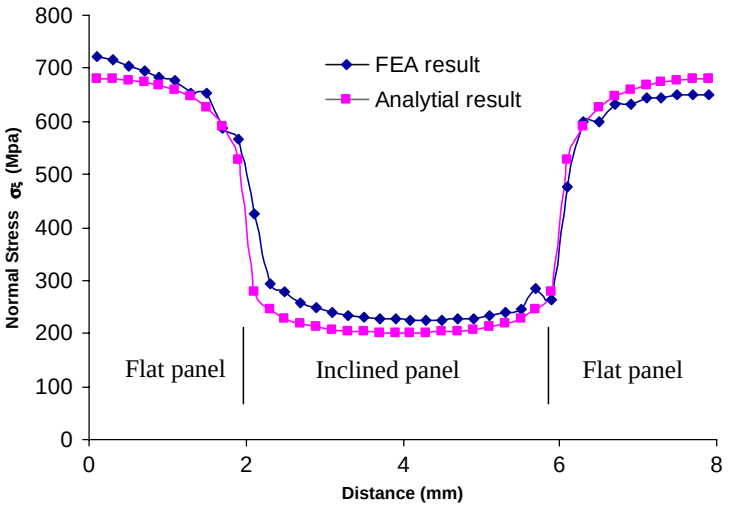

Fig. 27. Interfacial normal stress distribution: $\varepsilon_x^0 = 0.01$.

corresponding uniform strains $\varepsilon_x^0 = 0.01$ and $\varepsilon_y^0 = 0.01$. The distance is represented by the contour coordinate, from 0 to 2 mm and from 6 to 8 mm for the flat panel, and from 2 to 6 mm for the inclined panel (see Fig. 24). From Fig. 26–29, we can see that there is a good correlation between the FE and the present analytical results, which show the accuracy of the model derived in this study. It is interesting to note from Figs. 26 and 28 that shear stress arises due to the in-plane stretch and reaches its maximum at the panel-intersection and diminishes towards the center of the cell wall. From Fig. 27 we can observe that the force in the x-direction is carried mainly by the flat wall, whereas from Fig. 29, the force in the y-direction is carried mainly by the inclined wall.

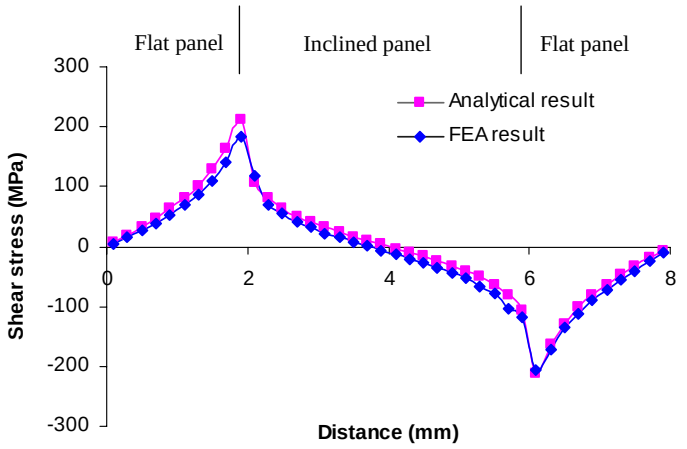

Fig. 28. Interfacial shear stress distribution: $\varepsilon_y^0 = 0.01$.

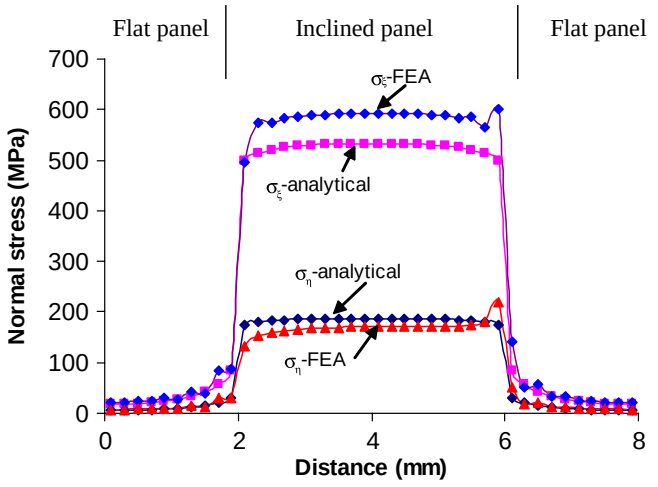

Fig. 29. Interfacial normal stress distribution: $\varepsilon_y^0 = 0.01$.

5.4. Application

Using the closed-form solution derived in this study, a parametric study is carried out for the interfacial shear stress at the corners. From Fig. 30, we can observe that S_{12} decreases as the aspect ratio increases, and S_{12} approaches zero when the height reaches infinity. This is in agreement with a previous study, which stated that as h approaches infinity, an hexagonal core in regard of its in-plane properties can be treated as being an isotropic continuum (Gibson and Ashby, 1988). We further note that since no tension force occurs at the interface, the stress-state of the core panels under in-plane stretching is less critical than that under transverse shear.

5.5. Summary and discussion for in-plane behavior

A closed-form solution is presented to study the in-plane behavior of sandwich core walls considering skin effect. From the above results, the following conclusions can be drawn:

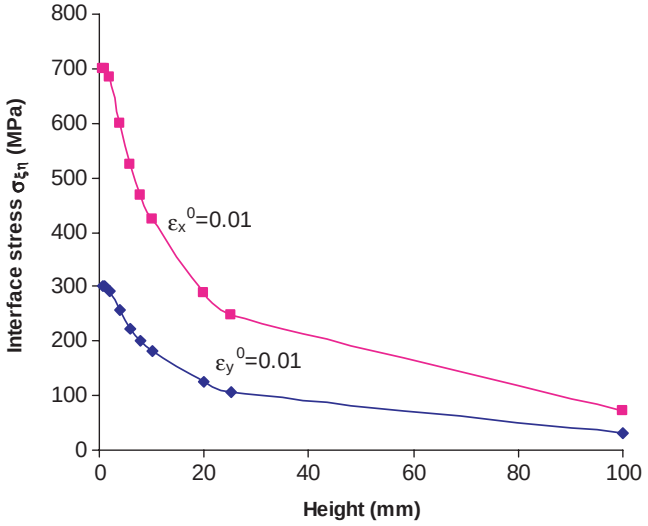

Fig. 30. Interfacial shear stress vs. core height.

1. Since the solution is based on equilibrium equations, it can predict both the stiffness and interfacial stress distribution. Unlike existing solutions (Becker, 1998), the present formulation is explicit and easy to implement, and in agreement with existing results, it can accurately model the in-plane stiffness.
2. The accuracy of this solution is verified through close correlations between FE and analytical results, both in terms of stiffness and interfacial stresses.
3. Additional shear stress arises at the interface due to skin effect under in-plane stretching. An apparent stress concentration can be observed at the corner of panel-intersection, making this location critical in design.
4. Interfacial shear stress is highly dependent on the skin effect, but as a function of the height, with the stress approaching zero when the core height becomes infinity.

6. Conclusions

This study is focused on developing an analytical model that permits the computation of stiffnesses as well as interfacial stresses considering the skin-effect for hexagonal honeycomb sandwich, subjected to in-plane and out-of-plane forces. An explicit analytical model is derived based on equilibrium equations, where boundary conditions imposed by the skin effect are appropriately considered. From this study, we can conclude:

1. The analytical solution can successfully predict the behavior of panels, accounting for the warping effect exerted by the outer skins, both in terms of stiffness and stresses, as verified by FE results.
2. The skin effect is a localized phenomenon. The lower bound of the equivalent stiffness can thereby be adopted if the aspect ratio is high enough, and it is suggested that the solution provided in this study be adopted when the aspect ratio is low in order to more accurately model the structure. However, the skin effect can significantly affect interfacial stress distribution, yielding a coupled stress state: a normal stress arises for transverse shear and a shear stress results from in-plane stretching. There is an

apparent stress concentration at the panel corners, making this location potentially critical in design. For in-plane stretching, the tensile stress is caused mainly by Poisson's effect and is less significant than that caused by transverse shear, and therefore, the out-of-plane shear behavior becomes more important when considering interfacial stresses.

3. The skin effects described herein affect the stress distribution of both the flat and inclined panel, due to the open cell configuration. This effect on the stress distribution becomes less significant in areas away from the interface.
4. A parametric study is carried out on the interfacial shear stress: when the height approaches infinity, the tensile stress approaches an asymptotic constant value under transverse shear, and the shear stress becomes zero under in-plane stretching. The relationship between interfacial stresses and aspect ratio is given, which can be used for the optimization of cell configurations.
5. The results provided in this study for interfacial shear stress, when combined with flatwise tension test results, can be used for failure predictions.
6. It should be noted that the other stiffness components, such as G_{xy}, G_{yz}, and E_{zz} are not affected by the skin effect, and they can be easily obtained. Thus, a complete set of stiffness prediction equations is available for computational models of orthotropic hexagonal sandwich panels.

Acknowledgement

Partial financial support for this study was received from the National Science Foundation Partnerships for Innovation program and the West Virginia University Research Corporation. We thank the reviewers of this paper for their constructive suggestions.

References

ABAQUS User's Manual (version 6.2) 2001. HKS, Inc., RI, USA.

Adams, R.D., Maheri, M.R., 1993. The dynamic shear properties of structural honeycomb materials. Composite Science and Technology 47, 15–23.

Allen, H.G., 1969. Analysis and Design of Structural Sandwich Panels. Pergamon Press, Oxford.

Becker, W., 1998. The in-plane stiffness of a honeycomb core including the thickness effect. Archives of Applied Mechanics 68, 334–341.

Burton, W.S., Noor, A.K., 1997. Structural analysis of the adhesive bond in a honeycomb core sandwich panel. Finite Element in Analysis and Design 26, 213–227.

Chen, A., Davalos, J.F., 2003. Bending strength of honeycomb FRP sandwich beams with sinusoidal core geometry. In: Proceedings of the Fourth Canadian-International Composites Conference, CANCOM 2003, Ottawa, Canada, August 19–22.

Chen, A., Davalos, J.F., 2004. Behavior of honeycomb FRP sandwich sinusoidal core panels with skin effect. In: Proceedings of 9th ASCE Aerospace Division International Conference on Engineering, Construction and Operations in Challenging Environments, Houston, TX, March 7–10, 2004. pp. 625–632.

Daniel, M.E., Abot, L.J., 2000. Fabrication, testing and analysis of composite sandwich beams. Composite Science and Technology 60, 2455–2463.

Davalos, J.F., Qiao, P., Xu, F.X., Robinson, J., Barth, K.E., 2001. Modeling and characterization of fiber-reinforced plastic honeycomb sandwich panels for highway bridge applications. Composite Structures 52, 441–452.

Fairbairn, W., 1849. An Account of the Construction of the Britannia and Conway Tubular Bridges. John Weale, London.

Fortes, M.A., Ashby, M.F., 1999. The effect of non-uniformity on the in-plane modulus of honeycombs. Acta Materiala 47 (12), 3469–3473.

Gibson, J.L., Ashby, M.F., 1988. Cellular, Solids Structure and Properties. Pergamon Press, Oxford.

Grediac, M., 1993. A finite element study of the transverse shear in honeycomb cores. International Journal of Solids and Structures 30 (13), 1777–1788.

Hohe, J., Becker, W., 2001a. A refined analysis of the effective elasticity tensors for general cellular sandwich cores. International Journal of Solids and Structures 38, 3689–3717.

Hohe, J., Becker, W., Goswami, S., 2001b. Singular stress fields in cellular cores for structural sandwich panels. Composite Structures 53, 9–19.

Hohe, J., Becker, W., 2001c. Assessment of the delamination hazard of the core face sheet bond in structural sandwich panels. International Journal of Fracture 109, 413–432.

Kelsey, S., Gellatly, R.A., Clark, B.W., 1958. The shear modulus of foil honeycomb cores. Aircraft Engineering 30, 294–302.

Masters, I.G., Evans, K.E., 1996. Models for the elastic deformation of honeycombs. Composite Structures 35, 403–422.

Noor, A.K., Burton, W.S., Bert, C.W., 1996. Computational models for sandwich panels and shells. Applied Mechanics Review ASME 49 (3), 155–199.

Penzien, J., Didriksson, T., 1964. Effective shear modulus of honeycomb cellular structure. AIAA Journal 2 (3), 531–535.

Shi, G., Tong, P., 1995. Equivalent transverse shear stiffness of honeycomb cores. International Journal of Solids and Structures 32 (10), 1383–1393.

Vinson, J.R., 1999. The Behavior of Sandwich Structures of Isotropic and Composite Materials. Technomic Publishing Company Inc., Pennsylvania, USA.

Warren, W.E., Kraynik, A.M., 1987. Foam mechanics: the linear elastic response of two-dimensional spatially periodic cellular materials. Mechanics and Materials 6, 27–37.

Xu, F.X., Qiao, P., 2002. Homogenized elastic properties of honeycomb sandwich with skin effect. International Journal of Solids and Structures 39, 2153–2188.

Xu, F.X., Qiao, P., Davalos, J.F., 2001. Transverse shear stiffness of composite honeycomb core with general configuration. Journal of Engineering Mechanics 127 (11), 1144–1151.

Zenkert, D., 1995. An Introduction to Sandwich Construction. Chamelon Press, London.